МАТЕМАТИЧНІ МОДЕЛІ СИГНАЛІВ ТА СИСТЕМ

UDC 621.391:519.22 DOI: https://doi.org/10.15407/vidbir2023.51.023

ADVANTAGES OF PERIODIC NON-STATIONARY RANDOM PROCESS MODEL IN VIBRATION SIGNALS PROCESSING

I. M. Javorskyj [1, 2], R. M. Yuzefovych [1, 3], O. V. Lychak [1], B. R. Komarnytskyi [1]

[1] H. V. Karpenko Physico-Mechanical Institute of the NAS of Ukraine, Lviv;

[2] Bydgoszcz University of Sciences and Technology, Bydgoszcz, Poland;

[3] Lviv Polytechnic National University, Lviv

E-mail: roman.yuzefovych@gmail.com

The use of two different techniques for the analysis of vibration signals, whose carrier harmonics are modulated by high-frequency narrow-band random processes is discussed. Periodically non-stationary random processes (PNRP) are suitable models for description of vibration signals of damaged mechanism. A proposed processing technique can be considered as an alternative to squared envelope analysis, kurtosis techniques, squared envelope spectrum and its use in the analysis of a vibration signal is discussed. It is shown that the spectral estimates obtained by the envelope square method are biased and inconsistent. The possibility of obtaining of the unbiased estimates by the PNVP method even for a signal/noise ratio equal to 0.07 has been demonstrated.

Keywords: *periodically non-stationary random processes, high-frequency modulations, analytic signal, squared envelope, kurtosis, vibration.*

ПЕРЕВАГИ МОДЕЛІ ПЕРІОДИЧНО НЕСТАЦІОНАРНОГО ВИПАДКОВОГО ПРОЦЕСУ ПІД ЧАС ОБРОБКИ ВІБРАЦІЙНИХ СИГНАЛІВ

І. М. Яворський [1,2], Р. М. Юзефович [1,3], О. В. Личак [1], Б. Р. Комарницький [1]

[1] Фізико-механічний інститут ім. Г. В. Карпенка НАН України, Львів;

[2] Бидгощська Політехніка, Бидгощ, Польща;

[3] Національний університет “Львівська політехніка”

Продемонстровано використання двох різних методів – періодично нестаціонарних випадкових процесів (ПНВП) та квадрата огинаючої для аналізу реальних вібраційних сигналів, несучі гармоніки яких модулюються взаємостаціонарними високочастотними вузькосмуговими випадковими процесами. ПНВП є адекватними моделями для опису сигналів вібрації пошкодженого механізму. У перших наукових працях основним інструментом виявлення несправностей був метод аналізу квадрата огинаючої, який використовують дотепер. Наведена методика ПНВП-аналізу сигналу є альтернативою до методу аналізу квадрата огинаючої та методу спектрального ексцесу. Численні результати, отримані шляхом обробки реальних вібраційних сигналів, підтвердили ефективність цієї моделі для опису саме тих характеристик вібрації, які є суттєвими для вирішення задач діагностики. Величини, які описують періодичну структуру моментних функцій першого та другого порядків для моделі ПНВП, є симптоматичними для виявлення дефектів, у т.ч. і на початкових стадіях їх розвитку. Зв’язок між аналізованими підходами схематично обговорювався, проте слід звернути увагу на їхню різну методологічну основу, що зумовлює відмінності в процедурах обробки сигналів, їх ефективності та інтерпретації результатів, пошуку засобів їх покращення. У межах ПНВП-підходу не визначається “квадрат огинаючої” як сума квадратів сигналу та його перетворення Гільберта, оскільки ця сума є високочастотним випадковим процесом, середнє якого дорівнює подвоєній дисперсії вхідного сигналу, а спектр “квадрата огинаючої” є спектром дисперсії з подвійною амплітудою. Показано, що спектральні оцінки, отримані методом квадрата огинаючої є зміщени-

ми і неслушними. Продемонстровано можливість отримання незміщених оцінок методом ПНВП навіть за відношення сигнал/шум, рівного 0,07.

Ключові слова: *періодично нестаціонарні випадкові процеси, високочастотні модуляції, аналітичний сигнал, квадрат огинаючої, ексцес, вібрація.*

Introduction. The techniques for analysis of vibration signals which are based on their model in the form of PNRP are known for years [1–5]. Numerous results, which have been obtained by processing real vibration signals confirmed the effectiveness of this model to describe exactly these features of signal that are essential to diagnose the mechanisms. The quantities, which describes the periodical structure of the first and second order moment functions for the PNRP model are well-applicable for fault detection in mechanisms. The first attempts to develop this approach were proposed in the second half of the 1990s [6, 7]. The squared envelope technique was the main tool for fault detection at that time [8–10] and is still widely used today. The relation between these approaches was discussed in brief in [11], underlining their different methodological bases, that is, the differences in their processing procedures, efficiency, and the idea of interpretation of results, searching for the means of improving their quality, etc. We cannot define "squared envelope" as the sum of squares of the raw signal and its Hilbert transform, because this sum is just the high-frequency random process, the mean function of which is equal to the doubled PNRP variance. In addition, the "squared envelope" spectrum is the doubled variance amplitude spectrum. The covariance function of the latter is equal to the fourth moment function of PNRP, which in spectral form is used for selecting the so-called "informative frequency band".

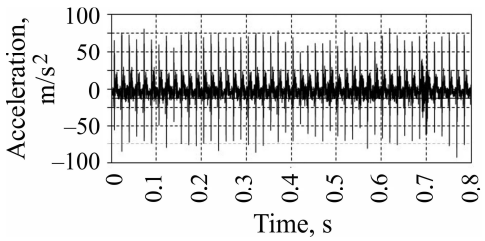

Fig. 1. Segment of the vibration signal.

Vibration signal and its characteristics. Mentioned above techniques were used to analyze the vibration signal of a decanter Flottweg 24E bearing unit. The vibration acceleration signals were acquired and pre-processed using the original data collection system. The accelerometer was fixed at the bearing unit casing. Cut-of frequency of an input signal filter was set 5 kHz, the sampling frequency was f_s = 10 kHz. Signal was collected du ring T = 10 s. A segment of collected signal is shown in Fig. 1.

To study the general properties of the collected vibration signal, the estimators of its covariance function and the power spectral density for stationary approximation of PNRP were calculated:

$$\hat{R}(jh)=\frac{1}{K}\sum_{n=0}^{R-1}\left[\xi(nh)-\hat{m}\right]\left[\xi\left((n+j)h\right)-\hat{m}\right], \quad \hat{m}=\frac{1}{K}\sum_{n=0}^{K-1}\xi(nh), \tag{1}$$

$$\hat{f}(\omega)=\frac{h}{2\pi}\sum_{n=-L}^{L}k(nh)\hat{R}(nh)\cos\omega nh. \tag{2}$$

Here, $h=T/K$ is the sampling interval; j is the integer number; T is the signal duration; K is the sample size, $L=u_m/h$; u_m is the cut-off point of the correlogram and $k(nh)$ is the covariance window.

Graphs of the covariance function and spectral density estimators are shown in Fig. 2. The undamped tail in the covariance estimator (Fig. 2*a*) induces the discrete component of the spectral density estimator – well-detectable peaks at certain frequencies These peaks could also be a result of the narrow-band stochastic modulation of the

carrier harmonics. Such mixed spectrum makes it difficult to interprete, evaluate and quantitative analyze the spectral estimation results, because it is necessary to separate the continuous components from discrete and to perform their individual analysis by means of suitable techniques. This is an important diagnostic issue, since the discrete and continuous components may be caused by different kinds of faults.

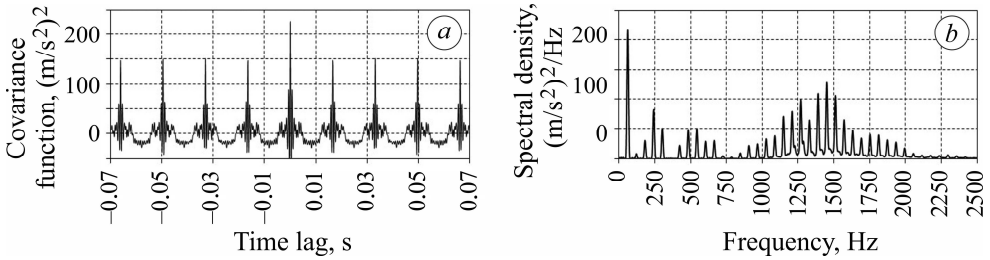

Fig. 2. Estimators of the covariance function (*a*) and the power spectral density (*b*) for signal stationary approximation.

We use the following functional [12, 13] to estimate of the period of the PNRP mean function, which describes the deterministic components in vibration signal:

$$\hat{F}_1(\theta)=\frac{1}{2K+1}\sum_{n=-K}^{K}\hat{m}^2(\theta,nh), \tag{3}$$

where

$$\hat{m}(\theta,nh)=\sum_{k=1}^{L_1}\left[\hat{m}_k^c(\theta)\cos k\frac{2\pi}{\theta}nh+\hat{m}_k^s(\theta)\sin k\frac{2\pi}{\theta}nh\right], \tag{4}$$

$$\begin{Bmatrix}\hat{m}_k^c(\theta)\\ \hat{m}_k^s(\theta)\end{Bmatrix}=\frac{2}{2K+1}\sum_{n=-K}^{K}\xi(nh)\begin{Bmatrix}\cos k\frac{2\pi}{\theta}nh\\ \sin k\frac{2\pi}{\theta}nh\end{Bmatrix}, \tag{5}$$

and θ is the test period. The possible errors caused by aliasing effects can be avoided by setting the sampling step h in (4) and (5) to satisfy the following inequalities [12]

$$h\le\frac{P}{2L_1+1},\qquad h\le\frac{P}{2L_2+1},$$

here L_1 and L_2 are the numbers of the highest harmonics, used for the mean and the covariance function estimations, respectively.

The maximum point of the functional (3) frequency dependence represents the basic frequency ($\hat{f}_0=1/\hat{P}$); within an accuracy of three decimal places. We find $\hat{f}_0=60.43$ Hz for our collected signal.

PNRP and SES analysis of the decanter vibration signal. Selection of the appropriate central frequency and the bandwidth is crucial in the squared envelope analysis method. Spectral kurtosis is one of the most powerful techniques for selection of the proper frequency band [14]. It was calculated using the equation

$$K_\xi(f)=\frac{\hat{S}_{4\xi}(f)}{\hat{S}_{2\xi}^2(f)}-2.$$

The statistic $\hat{S}_{2n\xi}(f)$ is the second-order empirical spectral moment defined as

$$\hat{S}_{2n\xi}(f)=\left\langle \left|F_W(kM,f)\right|^{2n}\right\rangle_k,$$

where $F_W(kM,f)$ is the so-called short-time Fourier transform

$$F_W(kM,f)=\sum_{n=k}^{k+K_W-1}\xi(nh)\,W(n-kM)\,e^{-i2\pi fn},$$

where $W(n)$ is the rectangular window of the length K_W and the sign $\langle\cdot\rangle_k$ marks the time-averaged operator over index k. Here it is assumed, that signal is locally stationary and the signal correlation length is shorter than the window length [11]. It is recommended in the literature to choose a window length somewhat shorter than the signal pulse width.

The local stationarity of the vibration signal condition is satisfied if the signal correlation length is much shorter than the non-stationarity period. This condition is rarely fulfilled for real vibration signals, but the spectral kurtosis is still successfully used in practice. In our case, the vibration signal also is not locally stationary, since the non-stationarity period is much shorter than the correlation length of the signal.

Since the largest part of power of the signals stochastic part is within the frequency range [0, 2.8 kHz] (see Fig. 2), we calculated the kurtosis for the frequencies which belong to this band. The window lengths were chosen as 0.3*P*, 0.4*P* and 0.6*P*. The largest values of the kurtosis are reached for $K_W=0.3P$ in the interval [0.2 kHz, 2.8 kHz] (Fig. 3).

To calculate the squared envelope spectrum, it is recommended to choose the frequency band around the central frequency with bandwidth equal 3 to 4 times of the basic frequency value [8, 15, 16]. We calculated the squared envelope spectrum selecting the band [1.3 kHz, 1.6 kHz], which contains 5 high-frequency components of the signal.

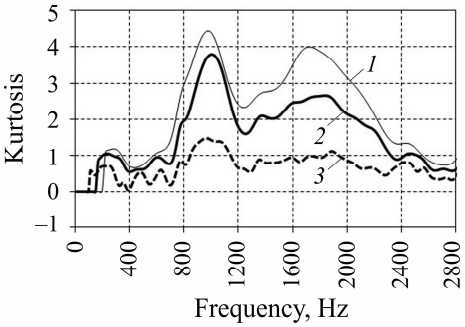

Fig. 3. Spectral kurtosis of the vibration signal: *a* – K_W = 0.3*P*; *b* – K_W = 0.4*P* and *c* – K_W = 0.6*P*.

The squared envelope spectrum is found using the discrete Fourier transform (DFT) of the squared modulus of the analytic signal [17]:

$$\mathrm{SES}(k)=\mathrm{DFT}\left\{\left|\zeta(n)\right|^2\right\}=\mathrm{DFT}\left\{\xi^2(nh)+\eta^2(nh)\right\}.$$

The discrete Fourier transform for squared envelope [18, 19]

$$\mathrm{DFT}\left\{\left|\zeta(n)\right|^2\right\}=\sum_{n=0}^{K-1}\left|\zeta(n)\right|^2 e^{-ik\frac{2\pi}{K}n}$$

is calculated using discrete-time Fourier transform [16, 20]

$$\hat{F}(f)=h\sum_{n=0}^{K-1}\left|\zeta(nh)\right|^2 e^{-i2\pi fnh}, \tag{6}$$

setting $f=k\Delta f$, $\Delta f=\frac{1}{Kh}$ and $\mathrm{DFT}\left\{\left|\zeta(n)\right|\right\}=\frac{\hat{F}(k\Delta f)}{h}$.

Taking into account $E\eta^2(nh)=E\xi^2(nh)$, the mathematical expectation of (6) will be

$$E\hat{F}(f)=2h\sum_{n=0}^{K-1}b_\xi(nh,0)e^{-i2\pi fnh}. \tag{7}$$

Substituting into (7) the dependence for the variance $b_\xi(nh,0)$ in the form of a Fourier series, we get

$$E\hat{F}(f)=2h\sum_{r=-2L}^{2L}B_r^{(\xi)}(0)e^{i\pi(rf_0-f)(K-1)h}\frac{\sin\pi(2f_0-f)Kh}{\sin\pi(rf_0-f)h}. \tag{8}$$

The values in (8) at points $f=rf_0$ are equal to:

$$E\hat{F}(rf_0)=2TB_r^{(\xi)}(0),$$

where $T=Kh$ is the signal duration time. So, the values $E\hat{F}(rf_0)\neq 2B_2^{(\xi)}(0)$ are different, depending on time.

The variance for (8) for Gaussian PNRP is equal to:

$$\mathrm{Var}\hat{F}(f)=4h^2\left[\sum_{n=0}^{K-1}\left[\begin{matrix}b_\xi^2(nh,0)+\\+b_{\xi\xi}^2(nh,0)\end{matrix}\right]+2\sum_{r=1}^{K-1}\sum_{n=0}^{K-r-1}\left[\begin{matrix}b_\xi^2(nh,0)+\\+b_{\xi\xi}^2(nh,rh)\end{matrix}\right]\cos 2\pi frh\right]. \tag{9}$$

As it follows from (9), $\mathrm{Var}\hat{C}(f)\to\infty$ as $K\to\infty$. So, such estimator is inconsistent and establishing properties of the estimator in (6) leads to significant errors in calculating the spectrum of the variance for the analytic signal using DFT.

Such inferences are confirmed by the processing results. In Fig. 4 the graphs of the frequency dependence of the value $\left|\hat{F}(f)\right|$ for the different realization lengths are presented. Here the values of $\left|\hat{F}(f)\right|$ were calculated with step $\Delta f=0.1$ Hz. Table 1 gives the maximum values of $\left|\hat{F}(f)\right|$. As we can see, the maximum values are changing approximately in proportion to the realization length, and the power of the fluctuations increases as the realization length grows. It is clear that in this case the maximum values cannot be considered as the estimators for the amplitudes of the squared envelope harmonics, while the points of the maximum values are close to the values of the basic frequency and its multiples.

Now introduce the transforms

$$\left\{\begin{matrix}\hat{C}_a(f)\\\hat{S}_a(f)\end{matrix}\right\}=\frac{2}{2K+1}\sum_{n=-K}^{K}\left[\xi^2(nh)+\eta^2(nh)\right]\left\{\begin{matrix}\cos 2\pi fnh\\\sin 2\pi fnh\end{matrix}\right\}, \tag{10}$$

which referred to as the component [21] or cyclic [22] statistics. SES is presented also in a similar form in [23, 24]. Based on the results of [25, 26], we can deduce that

$$\lim_{T\to\infty} C_a(f)=\begin{cases}2C_k(0), & f=kf_{0,}\\ 0, & \text{otherwise,}\end{cases}$$

$$\lim_{T\to\infty} S_a(f)=\begin{cases}2S_k(0), & f=kf_0,\\ 0, & \text{otherwise,}\end{cases}$$

and

$$\lim_{T\to\infty} \operatorname{Var} C_a(f)=0, \qquad \lim_{T\to\infty} \operatorname{Var} S_a(f)=0,$$

if the covariance components vanish as lag u increases:

$$\lim_{|u|\to\infty} B_r(u)=0, \qquad \forall r=\overline{0,2L}.$$

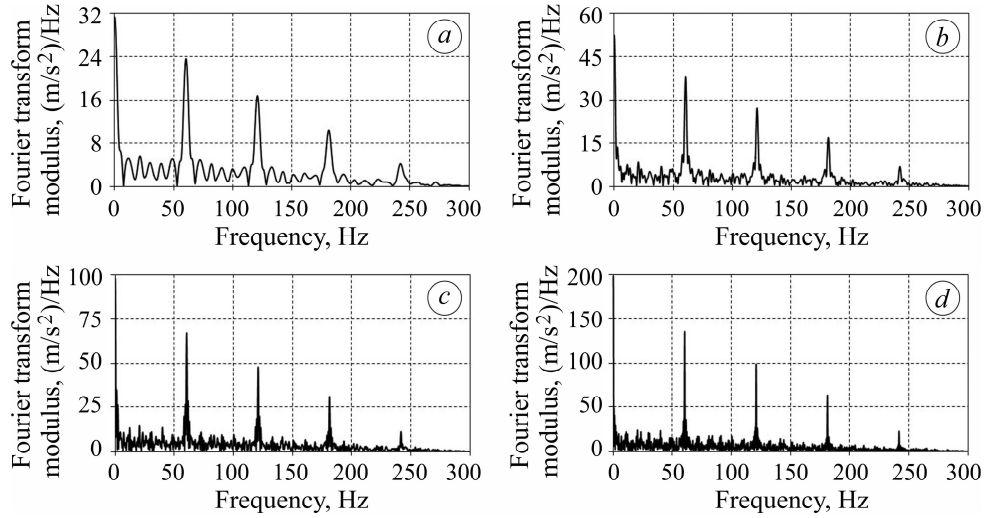

Fig. 4. Amplitude spectra of the analytic signal modulus:
a – $K = 3\cdot10^3$; *b* – $K = 6\cdot10^3$; *c* – $K = 12\cdot10^3$; *d* – $K = 24\cdot10^3$.

Table 1. Maximum values of Fourier transform (6) modulus and their points

Sample size, K	Maximum points, f_{max}, Hz				
	0	60.42	120.84	181.26	241.68
$3 \cdot 10^3$	31.238	23.559	16.823	10.388	4.073
$6 \cdot 10^3$	52.306	37.880	27.121	16.911	6.711
$12 \cdot 10^3$	97.696	67.220	47.960	30.871	11.052
$24 \cdot 10^3$	197.940	135.686	98.904	62.848	22.093

This means that the points of the extremums of statistic (6) can be considered as the estimators for carrier harmonics frequencies, and the extremum values – as the estimators of Fourier coefficients for analytic signal variance. The quantities $\hat{V}_a\left(k\hat{f}_0\right)=\left[\left[\hat{C}_a\left(k\hat{f}_0\right)\right]^2+\left[\hat{S}_a\left(k\hat{f}_0\right)\right]^2\right]^{1/2}$ can be considered as the estimators of harmonic amplitudes. It has been shown in [25, 26] that the variances of the frequency estimators have convergence order $\mathrm{O}(T^{-3})$, and the variance of the Fourier coefficient

estimators have convergence order $O(T^{-1})$. Taking this into account, we chose the estimation of the basic frequency f_0 as the first issue in the time series processing.

To detect the hidden periodicities of the second order, we use the variance functional [12, 13]

$$\hat{F}_2(0,\theta)=\frac{1}{2K+1}\sum_{n=-K}^{K}\hat{R}_\xi^2(nh,0,\theta). \tag{11}$$

As the next step, we calculated the variance Fourier coefficients using statistics (11) for $\theta=\hat{f}_0^{-1}$. The statistics obtained in this way, in contrast to (10), are selective only relative to harmonics with frequencies $k\hat{f}_0$ and their selectivities increase as the realization length grows.

The maximum values of $\hat{V}_a(f)=\left[\left[\hat{C}_a(f)\right]^2+\left[\hat{S}_a(f)\right]^2\right]^{1/2}$, which were calculated using cyclic statistics (10), are given in Table 2. For large K these values differ insignificantly from the values of the estimators for the variance Fourier coefficients.

Table 2. Maximum values of cyclic estimator $\hat{V}_a(f)$ for analytic signal modulus

Sample size, K	Maximum points, f_{max}, Hz				
	0	60.42	120.84	181.26	241.68
$3\cdot10^3$	104.163	157.114	112.188	69.278	27.158
$6\cdot10^3$	87.190	126.286	90.418	56.378	22.372
$12\cdot10^3$	81.420	112.042	79.940	51.456	18.420
$24\cdot10^3$	82.478	113.076	82.424	52.406	18.412

Unreasonable narrowing of the signal frequency band which is performed for calculating the squared envelope spectrum is one of the main disadvantages of this technique. It reduces the number of spectrum harmonics and thus, the estimated values of their amplitudes. As we can see, the filtered signal bandwidth must be three to four times as large as the traditionally chosen bandwidth. The wider frequency band makes it possible to involve a larger number of harmonics in the least square (LS) functional for discovering the hidden periodicities of the second order, and to improve its sensitivity. Note that we deal with a similar case analyzing vibrations which were selected from a wind turbine gearbox [13]. On the graph of the frequency dependence of the mono-component functional $\hat{C}_\xi(f)=\frac{2}{2K+1}\sum_{n=-K}^{K}\overset{\circ}{\xi}_0^2(n)\cos 2\pi fnh$, we can observe only chaotic oscillations (Fig. 5*a*), while the graph of the functional (11) for $L_2=10$ contains a clear peak (Fig. 5*b*) at the point $\hat{f}_0=24.2$ Hz that proves a defect initiation. The value of functional (11) at this point is $\hat{F}_2(\hat{f}_0)=338\cdot10^{-6}\ (\mathrm{m/s^2})^4$.

The time-averaged power of vibration is $\hat{B}_0(0)=223\cdot10^{-3}\ (\mathrm{m/s^2})^2$. If we define signal-to-noise ratio (SNR) as $\mathrm{SNR}=\frac{\hat{F}_2(\hat{f}_0)}{\hat{B}_0^2(0)}$ we obtain for our case $\mathrm{SNR}=0.07$. So, we can confirm that use of the LS functional (11) enables the fault detection for small enough SNR. This stage of the fault growth we can consider as initial.

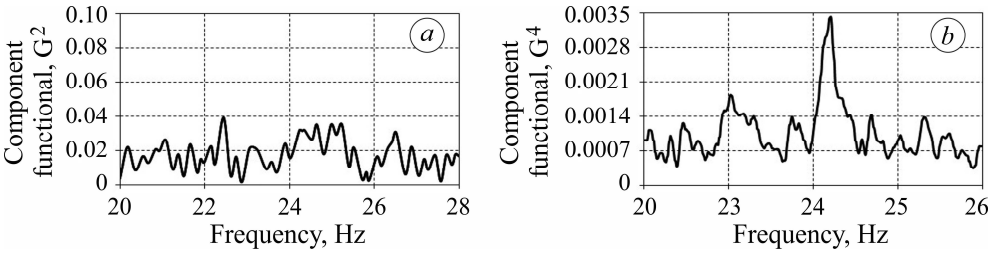

Fig. 5. Variance component (*a*) and LS functional (*b*) for gearbox vibration signal [12].

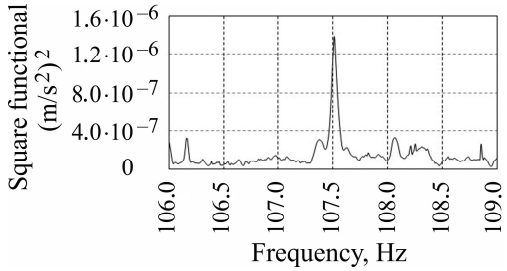

Fig. 6. Dependence of functional (11) on test frequency.

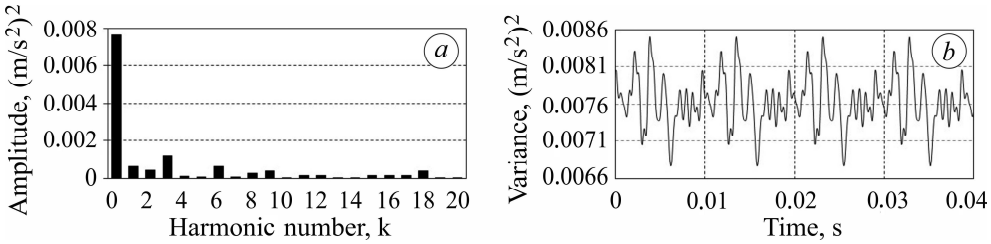

Fig. 7. Time changes of variance estimator (*a*) and their amplitude spectrum (*b*).

CONCLUSION

It has been shown that the square of the analytic signal modulus is not a “squared envelope” in the accepted sense, but is a random process, the mathematical expectation of which is equal to twice the variance of the raw signal. Hence, the Hilbert transform cannot be used as a demodulating procedure in this case, and the “squared envelope” can only be analyzed as a realization of a random process using PNRP techniques. The “squared envelope” spectrum used in the literature is naturally the amplitude spectrum of the time changes in the power for the stochastic part of the vibration. The issue of filtering of the raw signal for selection of the informative frequency band must also be re-formulated. It is necessary to consider it in terms of the filtering of a PNRP, which has some special features which must be taken into consideration for a more effective choice of bandwidth for the analysis.

1. Dragan Y.; Javorskyj I. *Rhythmics of sea waving and underwater acoustic signals*; Naukova Dumka: Kyiv, 1982 (in Russian).
2. Dragan, Ya.P.; Rozhkov, V.A.; Javorskyj, I.N. *Methods of probabilistic analysis of the rhythms of oceanological processes*; Hydrometeoizdat: Leningrad, 1987. (In Russian).
3. Gardner, W.A. *Cyclostationarity in Communications and Signal Processing*; IEEE Press: New York, 1994.
4. Hurd, H.L.; Miamee, A. *Periodically Correlated Random Sequences: Spectral Theory and Practice*; Wiley: New York, 2007. https://doi.org/10.1002/9780470182833
5. Antoni, J. Cyclostationarity by examples, *Mech. Syst. Signal Process.* **2009**, 23, 987–1036. https://doi.org/10.1016/j.ymssp.2008.10.010

6. Mykhailyshyn, V.; Javorskyj, I.; Vasylyna, Y.; Drabych, O.; Isaev, I. Probabilistic models and statistical methods for the analysis of vibration signals in the problems of diagnostics of machines and structures, *Materials Science*. **1997**, 33, 655–672. https://doi.org/10.1007/BF02537594
7. McCormick, A.C.; Nandi, A.K. Cyclostationarity in rotating machine vibrations, *Mech. Syst. Signal Process.* **1998**, 12, 225–242. https://doi.org/10.1006/mssp.1997.0148
8. McFadden, P.D.; Smith, J.D. Vibration monitoring of rolling element bearings by the high frequency resonance technique – A review. *Tribol. Int.* **1984**, 17, 3–10. https://doi.org/10.1016/0301-679X(84)90076-8
9. Ho, D.; Randall, R.B. Optimization of bearing diagnostic techniques using simulated and actual bearing fault signals. *Mech. Syst. Signal Process*. **2000**, 14, 763–788. https://doi.org/10.1006/mssp.2000.1304
10. Wang, H. Early detection of gear tooth cracking using the resonance demodulation technique. *Mech. Syst. Signal Process*. **2001**, 15, 887–903. https://doi.org/10.1006/mssp.2001.1416
11. Randall, R.B.; Antoni, J. Rolling element bearing diagnostics – A tutorial. *Mech. Syst. Signal Process*. **2011**, 25, 485–520. https://doi.org/10.1016/j.ymssp.2010.07.017
12. Javorskyj, I. *Mathematical models and analysis of stochastic oscillations*; Karpenko Physico-Mechanical Institute: Lviv, 2013. (in Ukrainian).
13. Javorskyj, I.; Matsko, I.; Yuzefovych, R.; Lychak, O.; Lys, R. Methods of hidden periodicity discovering for gearbox fault detection. *Sensors.* 2021, 21, 6138. https://doi.org/10.3390/s21186138
14. Antoni, J. The spectral kurtosis: A useful tool for characterising non-stationary signals. *Mech. Syst Signal Process*. **2006**, 20, 282–307. https://doi.org/10.1016/j.ymssp.2004.09.001
15. Antoni, J. Cyclic spectral analysis of rolling-element bearing signals: Facts and Fictions. *J. Sound Vib*. **2007**, 304, 497–529. https://doi.org/10.1016/j.jsv.2007.02.029
16. Abboud, D.; Elbadaoui, M.; Smith, W.A.; Randall, R.B. Advanced bearing diagnostics: A comparative study of two powerful approaches. *Mech. Syst. Signal Process.* **2019**, 114, 604–627. https://doi.org/10.1016/j.ymssp.2018.05.011
17. Tyagi, S.; Panigrahi, S.K. An improved envelope detection method using particle swarm optimisation for rolling element bearing fault diagnosis, *J. Comput. Des. Eng*., **2017**, 4, 305–317. https://doi.org/10.1016/j.jcde.2017.05.002
18. Kay, S.M. *Modern spectral estimation: Theory and application*. New Jersey: Prentice Hall, Englewood Cliffs, 1988.
19. Gardner, W.A. *Introduction to Random Processes with Applications to Signals and Systems*; Macmillan: New York, 1985.
20. Wang, D.; Zhao, X.; Kou, L-L.; Qin, Y.; Zhao, Y.; Tsui, K-L. A simple and fast guideline for generating enhanced/squared envelope spectra from spectral coherence for bearing fault diagnosis. *Mech. Syst. Signal Process.* **2019**, 122,754–768. https://doi.org/10.1016/j.ymssp.2018.12.055
21. Javorskyj, I.; Kravets, I.; Matsko, I.; Yuzefovych, R. Periodically correlated random processes: Application in early diagnostics of mechanical systems. *Mech. Syst. Signal Process*. **2017**, 83, 406–438. https://doi.org/10.1016/j.ymssp.2016.06.022
22. Napolitano, A. *Cyclostationary processes and time series: Theory, applications, and generalizations*; Elsevier, Academic Press., 2020.
23. Mauricio, A.; Smith, W.A.; Randall, R.B.; Antoni, J. Improved envelope spectrum via feature optimisation-gram (IESFOgram): A novel tool for rolling element bearing diagnostics under non-stationary operating conditions. *Mech. Syst. Signal Process*. **2020**, 144, 106891. https://doi.org/10.1016/j.ymssp.2020.106891
24. Antoni, J.; Borghesani, P. A statistical methodology for the design of condition indicators. *Mech. Syst. Signal Process.* **2019**, 114, 290–327. https://doi.org/10.1016/j.ymssp.2018.05.012
25. Javorskyj, I.; Yuzefovych, R.; Matsko, I.; Zakrzewski, Z. The least square estimation of the basic frequency for periodically non-stationary random signals. *Digit. Signal Process*. **2022**, 122, 103333. https://doi.org/10.1016/j.dsp.2021.103333
26. Javorskyj, I.; Dehay, D.; Kravets, I. Component statistical analysis of second order hidden periodicities. *Digit. Signal Process.* **2014**, 26, 50–70. https://doi.org/10.1016/j.dsp.2013.12.002

Received 04.09.2023